Review Article

URF PUBLISHERS
connect with research world

Journal of Artificial Intelligence, Machine Learning and Data Science

https://urfpublishers.com/journal/artificial-intelligence

Vol: 1 & Iss: 3

Image Feature Enhancement and Its Application in Fault Diagnosis of Rotating Machinery: A Review

Wei Wang[1] and Yongjian Sun[2]*

[1]School of Electrical Engineering, University of Jinan, Jinan, Shandong, China

*[2]School of Electrical Engineering, University of Jinan, Jinan, Shandong, China

Citation: Wang W, Sun Y. Image Feature Enhancement and Its Application in Fault Diagnosis of Rotating Machinery: A Review. *J Artif Intell Mach Learn & Data Sci*, 1(3), 86-99.

Received: 25 July, 2023; **Accepted:** 29 August, 2023; **Published:** 06 September, 2023

***Corresponding author:** Yongjian Sun, School of Electrical Engineering, University of Jinan, Jinan, Shandong, China. Email: sunyongjian2006@163.com

ABSTRACT

Rotating machinery plays an important role in industry. Fault diagnosis of rotating machinery can ensure the normal operation of industrial production. Using images to diagnose mechanical faults is a commonly used method. Therefore, some image enhancement techniques are useful for rotating machinery fault diagnosis. This review introduces the methods and principles of image enhancement. Firstly, the methods of image feature enhancement are described, and the applications of these methods in rotating machinery are listed. In addition, new image enhancement methods are summarized, including filter-based image enhancement, model-based image enhancement, and learning-based image enhancement. Finally, the trend toward image enhancement in the field of fault diagnosis is discussed. This review attempts to introduce more image feature enhancement and extraction methods for fault diagnosis, in order to provide some inspiration for researchers and promote the development of mechanical equipment fault diagnosis.

Keywords: image feature enhancement; fault diagnosis; rotating machinery; rolling bearing

Introduction

Image analysis is a commonly used diagnostic technique for identifying faults in mechanical equipment. For instance, when diagnosing bearings, a range of techniques can be employed such as spectral curve analysis, time domain waveform analysis, bifurcation diagram analysis, envelope spectrum analysis, and amplitude-frequency curve analysis to intuitively assess the condition of the bearing[1]. There are various methods for converting data into images. In the field of diagnosing mechanical faults, image analysis has proven to be effective[2]. The use of image analysis can effectively reduce noise compared to direct analysis of the original data[3]. Image analysis can identify the features of a fault and improve fault detection[4]. The accuracy of detecting mechanical surface cracks is directly impacted by the quality of image analysis technology[5]. Image feature information can be logically extracted more effectively than the original digital data[6].

Image-based statistical analysis has become the foundation for extracting significant feature information in various fields[7]. For instance, Dong et al. utilized image stitching algorithms and texture scanning of cable images to assess the degree of cable corrosion[8]. In the diagnosis of motor faults, Long et al. employed point symmetry mode[9]. Two-dimensional images are more effective at representing data compared to one-dimensional data, and extracting scale-invariant features from images enhances the detection of motor operation. Liu et al. used aerial images to diagnose insulators in power lines[10]. Ma et al. enhanced medical images to improve pathological diagnosis and automatic disease screening[11]. Yan et al. analyzed remote sensing images to detect the type and number of vehicles under various weather conditions[12]. Additionally, in the field of remote sensing, Zhao et al. studied the structural characteristics of remote sensing images and used them to generate accurate descriptions[13]. Therefore, image processing finds application in various fields. Historically, the methodology for image enhancement was

relatively straightforward; however, the resultant effects were unsatisfactory. For example, signal-converted images contain additional noise, while image blurring hinders feature extraction. Hence, the technology of image enhancement is continually evolving to better highlight the required features in an image using different methods.

Image enhancement is commonly used in fault diagnosis to denoise and reduce texture, effectively highlighting fault information and aiding in subsequent diagnosis. This technique employs specific methods to extract necessary information from the original image or suppress irrelevant details. Image feature enhancement primarily relies on techniques such as image denoising, segmentation, and fusion[14]. Pixel values are analyzed to achieve denoising for grayscale images or adjust colors for color images[15]. In fault diagnosis, gray-value images are frequently employed and commonly undergo processing using techniques such as gray-value transformation and histogram adjustment[16]. Color images contain more information compared to grayscale images[17]. In a color image, the value of a single pixel is determined not only by its grayscale value but also by the combination of multiple color components. Common color image models include RGB, HSV, HLS, and others[18]. An RGB image consists of the three primary colors: red, green, and blue[19]. HSV utilizes hue, saturation, and value components, while HIS incorporates hue, saturation, and intensity color structure. HSI outperforms RGB space in pixel recognition due to its richer and more discriminative spectral information. However, HSI suffers from spectral redundancy[20].

Currently, numerous image-based diagnostic methods are utilized. However, there has been a lack of systematic summarization of image fault feature enhancement methods by scholars. Therefore, this paper aims to facilitate the use of images for diagnosing rotating machinery by discussing various image feature enhancement methods such as filtering, template matching, gray level transformation, image fusion, and segmentation. The scope of this discussion is restricted to rotating machinery. Consequently, this review summarizes various image feature enhancement methods to improve the effectiveness of fault diagnosis in rotating machinery. The aim is to provide readers with valuable insights on diagnosing rotating machinery through the use of images.

The rest of the organization of this paper is as follows: in Section 2, we review the image enhancement technology, classify the image enhancement technology, and clarify the principle. In Section 3, the new methods of image enhancement are introduced from the aspects of denoising, model-based, and learning-based. The fourth section introduces the method of image fusion. In Section 5, the image processing method of image fusion is introduced. In Section 6, other potential directions in image enhancement are indicated.

Approaches of Image Feature Enhancement

In the field of fault diagnosis, numerous methods are employed to convert data into images. Fig.2 presents a compilation of images utilized in mechanical diagnosis, encompassing seven distinct types such as recurrence plots, synchronized dot patterns, Gramian Angular Fields, Markov transition fields, fast kurtograms, and Spectra. These methods involve mapping one-dimensional time series onto a two-dimensional space. Fault diagnosis is achieved by extracting image features[21]. Various signals result in distinct images after conversion. The objective of image feature enhancement is to enhance the differentiation between images, making it a significant research direction. Image feature enhancement serves as an effective processing method for fault types with diverse categories and limited features. Moreover, the primary objective of fault diagnosis for mechanical equipment is image classification. Consequently, the research focuses on image feature enhancement and classification.

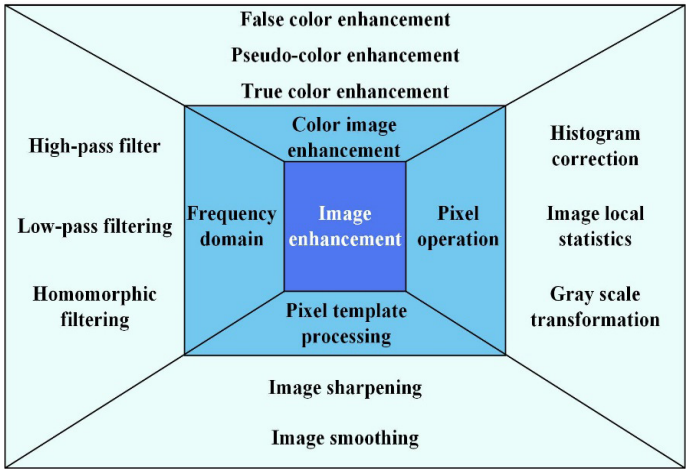

Figure 1: Classification of traditional image enhancement techniques

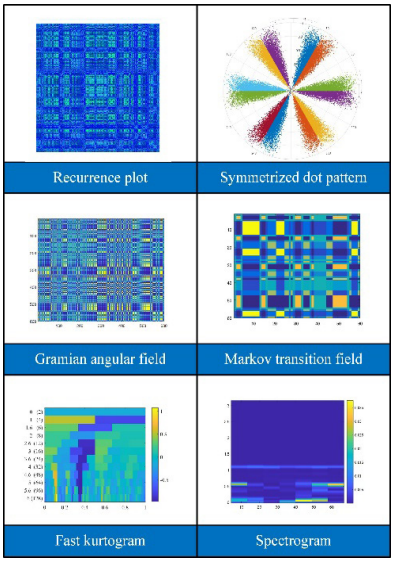

Figure 2: Six types of images are used in fault diagnosis

In the fault diagnosis of rotating machinery, these images contain a significant amount of signal information. The texture, color, and shape of the image can reflect various signal characteristics from different perspectives. Consequently, distinct images correspond to different signals, enabling the classification of mechanical signal faults. However, which image features better reflect the signal characteristics? What methods can be employed to enhance image processing? What are the key characteristics of image enhancement methods? These are significant research questions. The objective of image processing is to enhance diagnostic accuracy. Therefore, image enhancement represents a valuable research direction. Subsequently, this paper will discuss image enhancement methods from the perspectives of filtering, template creation, and grayscale transformation.

Image feature enhancement based on filtering

Image enhancement in the frequency domain requires the initial application of Fourier transform to the image. Subsequently, it is necessary to filter the transformed signal.

As depicted in Fig.3, the enhanced image is reconstructed by applying the inverse Fourier transform to the filtered signal.

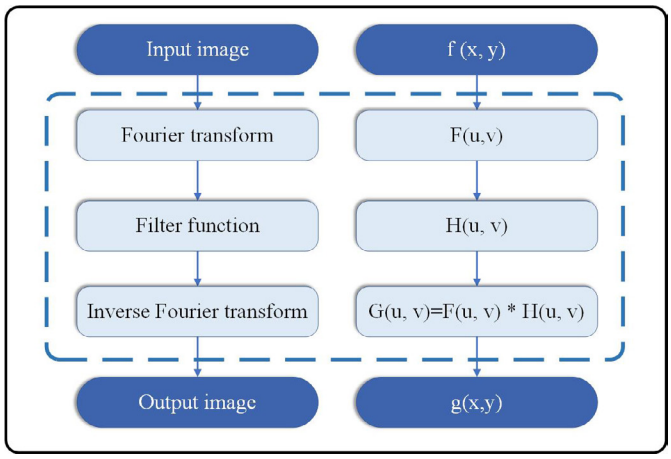

Figure 3: Frequency domain image enhancement flow chart

Noise in mechanical signals is typically concentrated in the high-frequency domain. Applying a low-pass filter to the Fourier-converted signal can effectively suppress and eliminate noise[22]. In computer vision, the high-frequency domain of the spectrum captures image texture details, whereas the low-frequency domain represents smooth regions. Figure 3 illustrates that altering the filtering function can result in diverse filtering effects. To filter the image signal, the converted signal is multiplied by the filtering function .

The eq.1 shows the definition of an ideal low-pass filter. Due to the low-pass filter's filtering mode only considering as the demarcation point, the filtering method is simplistic. In fault diagnosis, the high-frequency noise of the image can be effectively eliminated.

$$H(p,q) = \begin{cases} 1, & D(p,q) \le D_0 \\ 0, & D(p,q) > D_0 \end{cases} \qquad (1)$$

Where D_0 is the cutoff frequency and $D(p, q)$ represents the distance between the point (p, q) in the frequency domain and the image center in the frequency domain.

Eq.2 demonstrates the Butterworth low-pass filter (BLPF) function. The filtering effect varies depending on the chosen value for the filter order n. The filter boundary of the Butterworth low-pass filter is smoother than that of an ideal low-pass filter.

$$H(p,q) = \frac{1}{1+[D(p,q)/D_0]^{2n}} \qquad (2)$$

Where n is the order of the filter.

The Gaussian low-pass filter (GLPF) function is shown in eq.3, because the filter function is approximately Gaussian distribution, so the filter boundary is smoother and the high-frequency information will not be completely lost[23]. Compared with the above two filters, this one can better ensure the details of the image.

$$H(p,q) = e^{\frac{-D^2(p,q)}{2D_0^2}} \qquad (3)$$

Unlike the low-pass filter, the high-pass filter eliminates the low-frequency signal from the image while preserving the high-frequency component. The high-pass filter smooths out the image's smoother areas while preserving texture details. Eq.4 demonstrates the function of the ideal high-pass filter (IHPF), which retains the high-frequency components contrary to the ideal low-pass filter. In the diagnosis of surface details, the high-pass filter effectively filters the image background while preserving texture details like cracks. However, the removal of all high-frequency components can cause image distortion. The Butterworth high-pass filter (BHPF) and Gaussian high-pass filter (GHPF), complementary to their respective low-pass filters, can smooth the texture details in the filtered image. Eq.5 demonstrates the Butterworth high-pass filter function (BHPF), while eq.6 demonstrates the Gaussian high-pass filter function (GHPF). Among the three high-pass filters, the Gaussian high-pass filter provides the smoothest image outcome.

$$H(p,q) = \begin{cases} 0 & D(p,q) \le D_0 \\ 1, & D(p,q) > D_0 \end{cases} \qquad (4)$$

$$H(p,q) = \frac{1}{1+[D_0/D(u,v)]^{2n}} \qquad (5)$$

$$H(p,q) = 1 - e^{-D^2(p,q)/2D_0^2} \qquad (6)$$

By combining the aforementioned low-pass and high-pass filtering methods, homomorphic filtering is able to independently consider the low-frequency and high-frequency components of the image. Homomorphic filtering is a widely used approach capable of removing multiplicative noise. Furthermore, it enhances both contrast and brightness, thereby achieving image enhancement. Eq.7 demonstrates the homomorphic filtering function. The discrepancy in H_{hp} determines whether the image filtering is low-pass or high-pass, while the magnitude of γ determines the strength of the filtering.

$$H(p,q) = (\gamma_H - \gamma_L)H_{hp}(p,q) + \gamma_L \qquad (7)$$

Where γ_H represents the high frequency weight, γ_L represents the low frequency weight, and H_{hp} can be the above filtering function.

In the field of mechanical engineering, filtering is widely recognized as an effective method for noise elimination and feature enhancement. To assess the health condition of bearings, Kaya et al.[24] utilized eight distinct filters to eliminate noise and improve the accuracy of the classification algorithm. By processing the data with the aforementioned filters, the signal's features were extracted. Additionally, Wang et al.[25] introduced the low-pass filter and sparsity-based algorithm (LpfSpaA) to effectively separate feature fluctuations from noise in planetary gearboxes. Their proposed algorithm incorporates a low-pass filter, which facilitated the extraction of potential faults. Similarly, Zhang et al.[26] presented a novel unsupervised learning algorithm named fast intrinsic component filtering, which is adept at fault diagnosis in rotating machinery. Building upon this, Li et al.[27] devised a Gabor convolution filtering method with robustness demonstrated through bearing and gear datasets validation. The Gabor convolution filter effectively suppresses the attenuation of critical image features. Lastly, Zou et al.[28] developed the multi-scale weighted entropy morphological filtering technique, which possesses the ability to heighten the dissimilarity between various fault data classes while simultaneously reducing computational complexity. This filter manages to significantly decrease the learning cost while maintaining high classification accuracy.

In the diagnosis of mechanical parts for fault detection, different filtering methods yield varied effects owing to the presence of diverse surface texture defects. For instance, certain defects require distinguishing from the background texture, while others, being minute in size, necessitate filtering out a broad

range of background images to accentuate the defect features. Consequently, in image-based fault diagnosis, the primary objective of filtering lies in eliminating extraneous information while preserving detailed fault characteristics, as the quality of filtering directly impacts subsequent defect detection and fault diagnosis. To enhance the quality of welding images, Effat et al.[29] employed interlaced multi-level bilateral filtering and wavelet thresholding methods for image enhancement. This approach effectively reduces image noise and accentuates damage and defect features in welded joints, facilitating convenient fault diagnosis. In contrast to filtering methods in the spatial and frequency domains, bilateral filtering combines information from both domains, offering the advantage of retaining sharp edges while smoothing out details. The conversion formula for the bilateral filter at the pixel with position is presented in eq.8. Similarly, Tomasz utilized multi-stage filtering and entropy for processing gearbox vibration signals[30]. This method offers denoising capabilities, enabling the observation of clear symptoms of damage in the resulting denoised image.

$$\tilde{I}(x) = \frac{\sum_{x_i \in N(x)} I(x_i) e^{\left(-\frac{\|x_i - x\|}{2\sigma_d^2}\right)} e^{\left(-\frac{|I(x_i) - I(x)|^2}{2\sigma_r^2}\right)}}{C} \quad (8)$$

Where σ_d and σ_γ are controlling parameters in spatial and intensity domains. The value of c is as follows:

$$C = \sum_{x_i \in N(x)} e^{\left(-\frac{|I(x_i) - I(x)|^2}{2\sigma_T^2}\right)} e^{\left(-\frac{|I(x_i) - I(x)|^2}{2\sigma_r^2}\right)} \quad (9)$$

Where $N(x)$ is the spatial neighborhood of x. $I(x)$ represents the value of the pixel at the x position.

Various filtering effects can be achieved by adjusting the two parameters σ_d and σ_γ. For instance, reducing the spatial parameter σ_d can enhance image sharpness, while increasing the value of σ_γ can bring the bilateral filter closer to a Gaussian filter. In the diagnosis of welding images conducted by Effat, an increase in σ_d results in a decrease in the peak signal-to-noise ratio (PSNR) and a smoother output image. To further enhance the image, Effat incorporates the wavelet threshold filter in combination with the bilateral filter by decomposing the image into low and high frequencies and subsequently applying a multi-level filtering process. The synthesized enhanced image, represented in fig.4, enables more prominent visualization of defect outlines. This multilevel filtering approach enhances the clarity of defect regions in the image and mitigates background interference, facilitating easier fault diagnosis.

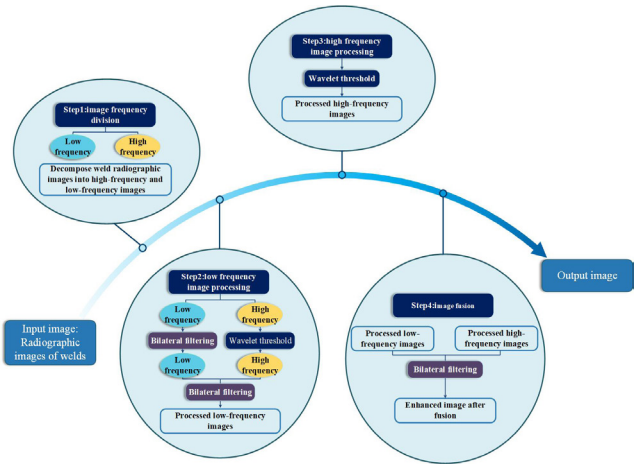

Figure 4: Multi-level Image Enhancement flowchart based on bilateral filtering and Wavelet threshold method

The aforementioned methods effectively enhance the visibility of fault textures in the field of fault diagnosis. Nonetheless, the calculation becomes time-consuming due to the multi-level image decomposition and filtering involved. To expedite the texture smoothing process in images, Ghosh et al.[31] devised an improved version of the bilateral filter that accelerates the computing speed by an order of magnitude while preserving the quality of the filter. The key principle revolves around modifying one of the Gaussian kernel functions employed in the original bilateral filter. By utilizing both Gaussian and box kernels, the computational efficiency is enhanced without significant visual discrepancies after image processing. As a result, the updated formula for the bilateral filter is exhibited in eq.10.

$$f_{BF}(i) = \frac{\sum_{j \in \Omega_i} \phi(f(j) - f(i)) f(j)}{\sum_{jen} \phi(f(j) - f(i))} \quad (10)$$

Where ϕ is a Gaussian range kernel, as shown below:

$$\phi(t) = exp\left(-\frac{t^2}{2\sigma^2}\right) \quad (11)$$

Where σ Controls the width of the scope core.

The improved bilateral filter is based on the classical bilateral filter and allows for control of the filtering effect through the parameter **σ**. A smaller value of **σ** results in less smoothing, while a very small value of **σ** essentially eliminates the filtering effect. Conversely, a larger value of **σ** leads to smoother edges. Within a certain range, the choice of **σ** can produce a desirable texture filtering effect in the image. Numerous methods have been developed to enhance the bilateral filter, such as modifying the filtering kernel function and incorporating additional algorithms. Table 1 lists some of these improved methods and their respective advantages.

In summary, different filtering methods can yield different effects, improving the edge and texture features of an image. Consequently, selecting an appropriate filter can accentuate specific characteristics in the signal.

Table 1. Improved method based on bilateral filter

No	Improved bilateral filter method	Advantage	Ref
1	Asymmetric bilateral exponential decay wavelet	Match the pulse characteristics in the vibration signal more flexibly	[32]
2	Bilateral filter and its variants in least Squares Framework	Fast operation speed and adaptability to different image types	[33]
3	Gaussian lifting framework for fast bilateral and non-local mean filtering	Runs fast and preserves the texture of the image well	[34]
4	Replace the bilateral filter of each pixel based on the weighted average of adjacent pixels	Improve spatial smoothness and reduce the influence of speckle noise	[35]
5	Fast bilateral filter based on intensity between pixels	Fast running speed, easy to expand to color images	[36]

Image feature enhancement based on template

In addition to processing individual pixels and adjusting the distribution of grayscale values, templates are employed to process both the pixels of an image and their adjacent pixels. A template functions as a filter by convolving the corresponding

pixels of the image using a template matrix. Consequently, the pixel value of the enhanced image depends not only on the original corresponding pixel but also on the grayscale value of the surrounding pixels. The template essentially serves as a convolution kernel, allowing for different effects like smoothing, filtering, and image sharpening when traversing across the entire image. Different templates yield varying outcomes in the processed images.

As an example, consider the neighborhood averaging method. In a 3 × 3 template, typically represented by eq.12, the purpose of this template is to average the grayscale values of the pixels in the *m*-th row and *n*-th column of the image with the eight surrounding pixels, subsequently assigning the calculated values to the pixels in the same row and column. Although this template offers the advantage of simple calculation, it falls short in effectively removing salt and pepper.

$$H = \frac{1}{9}\begin{bmatrix} 1 & 1 & 1 \\ 1 & 1 & 1 \\ 1 & 1 & 1 \end{bmatrix} \qquad (12)$$

When the template H is changed, namely, when altering the convolution operator, the image can be sharpened. Image sharpening serves to enhance the texture of the image, and different sharpening template operators can produce varying degrees of sharpness. Commonly used template operators include the Robert operator, Prewitt operator, Sobel operator, and others. Texture pixels typically possess notable distinctions from the surrounding pixel values, which can be expressed through the gradient along a specific direction. Once the image is transformed into a grayscale image, it can be considered as a two-dimensional matrix, divided into the row direction X and the column direction. The Robert operator, shown in eq.13, features a 2 × 2 convolution kernel. The Prewitt operator, shown in eq.4, and the Sobel operator, shown in eq.15, employ a 3 × 3 convolution kernel. Incorporating such symmetry ensures the preservation of the image's center point after processing[37].

$$R_x = \begin{bmatrix} 1 & 0 \\ 0 & -1 \end{bmatrix}, R_y = \begin{bmatrix} 0 & -1 \\ 1 & 0 \end{bmatrix} \qquad (13)$$

$$P_x = \begin{bmatrix} -1 & 0 & 1 \\ -1 & 0 & 1 \\ -1 & 0 & 1 \end{bmatrix}, P_y = \begin{bmatrix} 1 & 1 & 1 \\ 0 & 0 & 0 \\ -1 & -1 & -1 \end{bmatrix} \qquad (14)$$

$$S_x = \begin{bmatrix} -1 & 0 & -1 \\ -2 & 0 & 2 \\ -1 & 0 & 1 \end{bmatrix}, S_y = \begin{bmatrix} 1 & 2 & 1 \\ 0 & 0 & 0 \\ -1 & -2 & -1 \end{bmatrix} \qquad (15)$$

Where x represents the edge detection operator along the x-axis and y represents the edge detection operator along the y-axis.

Taking the Sobel operator as an example, the schematic diagram in Fig.5 displays the operation of the Sobel operator on the image. In this operation, the gradient value in a specific direction is obtained by computing the weighted sum of the gray values within the template region. The resulting gradient value from both directions represents the gray value of the pixel after passing through the template, as indicated by eq.16. Ammar et al.[38] employed the Sobel and Prewitt operators to segment the image. The fault diagnosis of an induction motor is achieved by dividing the region. Long et al.[39] utilized the Canny operator for texture detection and feature extraction of the wind turbine. The abnormal data from the wind turbine were statistically eliminated. Each operator yields different effects on various images due to the divergence in templates for each direction. For instance, the Robert operator offers accurate edge positioning and rapid processing speed due to its second-order matrix template. On the other hand, the Prewitt operator is able to suppress noise.

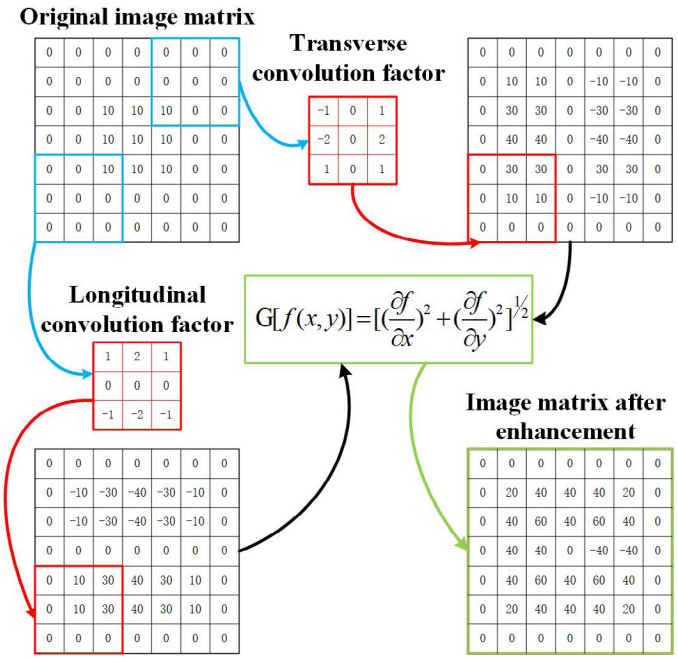

Figure 5: Enhanced image based on sobel operator template

$$G[f(x,y)] = [(\frac{\partial f}{\partial x})^2 + (\frac{\partial f}{\partial y})^2]^{1/2} \qquad (16)$$

where $\frac{\partial f}{\partial x}$ represents the gradient in the direction. $\frac{\partial f}{\partial y}$ represents the gradient in y direction.

Image feature enhancement based on model

In 1964, Edwin H. Land introduced the Retinex theory, which has become widely employed in the fields of machine vision and fault diagnosis. For instance, Chen et al. utilized the Retinex model to enhance images, thereby providing higher quality images for subsequent fault diagnosis of the current carrying ring. This model originates from human vision experiments, which have yielded several key findings[40]. Firstly, the retina processes different wavelengths of light separately, and the color of a given point is influenced by the colors surrounding it. Additionally, the edges play a significant role in color vision. By conducting pre-calibration, luminance calculation, and post-calibration on RGB images, the Retinex model effectively enhances the images. This model regards the image as a combination of the illuminating layer and the reflective layer, as depicted in eq.17.

$$S(x,y) = I(x,y) * R(x,y) \qquad (17)$$

where represents the illumination layer image, represents the reflection layer image, and represents the mixed image.

Compared to traditional linear and nonlinear methods, the model offers adaptive image enhancement. By dividing the image into two parts, the model effectively addresses the mixing of the illumination and reflection layers, eliminates image artifacts, and generates images with clear contrast and natural color. To further enhance the overall image quality, constraints can be added to the model based on specific objectives, such as emphasizing texture information, improving image exposure, and reducing image noise. For instance, the Single Scale Retinex (SSR) approach considers the lighting layer image, denoted as $I(x, y)$, as a low-frequency component. By applying low-pass filtering to the illuminated image layer, the essential image information can

be preserved. The decomposition formula of the SSR method is shown in eq.18. This method decomposes the image into two layers, where $F(x, y)$, represents the center surround function, which has a Gaussian-like form as depicted in eq.19. The center surround function captures the low-frequency part of the image. Filtering this low-frequency information results in only the high-frequency component remaining, enabling the model algorithm to retain the image's high-frequency information, including edge details. In the case of Multi Scale Retinex (MSR), it employs different Gaussian functions based on the SSR method. Multiple SSR images are then averaged to maintain high image fidelity.

$$I(x,y) = F(x,y) * S(x,y) \qquad (18)$$

$$F(x,y) = xe^{\frac{-(x^2+y^2)}{c^2}} \qquad (19)$$

Where c is a constant, and $F(x, y)$ is a central circumferential function.

The image enhancement method described above is based on the Retinex model, which utilizes a Gaussian filter to characterize the illumination layer of the image. However, it may not be suitable for all images. In order to enhance the model, various image enhancement effects can be achieved. Table 2 provides a list of different improvement methods based on the Retinex model.

Table 2. Image Enhancement method based on Retinex Model

No	Method	Advantage	Ref
1	Deep reflectance estimation network based on a Retinex variant	Adapt to more different lighting conditions and reduce color deviation	41
2	Combining exponentialized Mean Local Variance with Structure and Texture Aware Retinex (STAR) model	Extract precise structure and texture map	42
3	A local flatness based variational approach to Retinex	Correction of uneven illumination	43
4	A retinex-based decom-position model for a hazy image and a novel end-to-end imagedehazing network	Overstretching and understretching are realized by automatically adjusting the attention weight of channel direction and pixel direction	44
5	Retinex based detail preserving variational model	Decompose directly in the image domain to maintain image details	45

Based on the Single Scale Retinex method, Michela et al.[46] presented the Path-Based Milano Retinex Algorithm (PMRA) after studying the Milano Retinex family. This algorithm enables precise analysis of the local structure in both grayscale and color images. The main principle involves incorporating the calculation of pixel luminance intensity along a specific path, as depicted in eq.20.

$$L(x) = \frac{1}{n}\sum_{k=1}^{n} \prod_{t_k=1}^{l_k-1} \delta_k(R_{t_k}) \qquad (20)$$

Where R_{tk} is the ratio function of the intensity between pixels, and n is the number of pixels, δ_k is defined as follows:

$$\delta_k(R_{tk}) = \begin{cases} R_{tk} & if\ 0 < R_{t_k} \le 1-\varepsilon \\ 1 & if\ 1-\varepsilon < R_{t_k} < 1+\varepsilon \\ R_{tk} & if\ 1+\varepsilon \le R_{tk} \le \frac{1+\varepsilon}{\prod_{k=1}^{t_k-1}\delta_k(R_{m_k})} \\ \frac{1}{\prod_{m_{k-1}}^{t}\delta_k(R_{m_k})} & if\ R_{tk} > \frac{1}{\prod_{m_{k-1}}^{t}\delta_k(R_{m_k})} \end{cases} \qquad (21)$$

Where ε is the threshold.

The formulas in the third and fourth functions differ slightly from the original Retinex. The calculation method for pixel intensity along the path from x_1 to x_4 under the conditional equation δ_k is elucidated in fig.6.

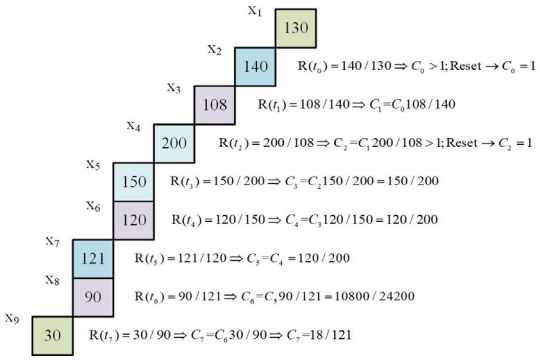

Figure 6: A method for calculating the luminance intensity of MR along the path[62]

From the conditional function, it can be observed that $\delta_k(R_{tk})$ equals 1 only when R_{tk} tends to 1. As shown in fig.6, the intensity ratio function R_{tk} =140/130>0 between x_1 and x_2 and , resulting in the resetting of to 0. On the other hand, R_{tk} =108/140<1 between $x_{2\,\text{nad}}x_3$, leading to C_1=108/140.

After conducting experiments, Michela et al. noted that the value of $L(x)$ is inversely proportional to the contrast of pixels at position x. Consequently, this model allows for the measurement of pixel-level contrast between two images. The eq.22 defines this contrast measure. After performing the necessary calculations, the pixel value of the smooth regions in the image is set to 0. However, in non-uniform areas, the value remains positive but less than 0. This algorithm highlights a significant correlation between contrast and luminance intensity $L(x)$. Since it is based on the Retinex algorithm, it effectively eliminates minor intensity fluctuations in the scene and reduces the impact of noise on contrast. Ultimately, this improves the performance of image retrieval in low-light environments.

$$MiRCo(x) = 1 - L(x), \forall x \in S \qquad (22)$$

Where $L(x) = \frac{1}{n}\sum_{k=1}^{n} \prod_{k=1,t=j_k}^{l_k-1} \delta(R_k(t))$, $\delta(R_k(t)) = \begin{cases} 1 & if\ 1-\varepsilon < R_k(t) \le 1+\varepsilon \\ R_k(t) & otherwise \end{cases}$, $R_k(t) = \frac{I(\gamma_k(t+1))}{I(\gamma_k(t))}$, I is the color channel of RGB image, γ_k represents the path.

Similarly, Zhou et al.[47] developed a low-light image enhancement algorithm by simplifying the Retinex model based on the low-light model. In this approach, the Max RGB technique is employed to estimate the illumination layer, while an edge-preserving filter is utilized to refine the image after applying MaxRGB. The model consists of two components: lighting-aware source generation and multi-source fusion. By processing the input image using this model, the visual naturalness, color distribution, and overall quality of the image are improved compared to both single and multi-source models. Moreover, Gu et al.[48] introduced a fractional-order variational model based on the Retinex model to enhance severe low-light images, as shown in eq.23. This enhanced model provides better filtering of the illuminating layer image, denoted as $I(x,y)$. Each model has its own suitable application in mechanical diagnosis, and selecting the appropriate model for image enhancement yields different effects. For instance, in low-light environments and mechanical crack or fault diagnosis, the chosen model produces

superior outcomes. In a separate study, Li et al.[49] employed a fast Deriche filter to improve the multi-scale Retinex method. They successfully applied this technology to contour extraction in diamond roller machines, achieving high precision in contour measurement.

$$\min E(R,L) = \frac{1}{2}\int_{\Omega}|IL-S|^2\,dx + \lambda_1\int_{\Omega}|\nabla^{\alpha}R|\,dx + \lambda_2\int_{\Omega}|\nabla^{\alpha}L|\,dx \quad s.t.\ \tau \le I \le 1, I \le L \le \frac{I}{\tau} \tag{23}$$

where τ is the lower limit of reflectivity. λ represents the regularization coefficient. α and β Is the fractional order parameter contained in the interval .

The Retinex model is extensively utilized in natural image processing. Due to its diverse array of models, it yields beneficial effects in enhancing image details and reducing image noise. This precisely aligns with the requirements of mechanical equipment diagnosis. The Retinex model offers superior processing capabilities for color images, which encompass more information compared to grayscale images. In fault diagnosis, a higher quantity of information translates to a greater number of features, which also yields advantages.

Image feature enhancement based on gray level transformation

In pixel processing, grayscale transformation is a common method used for image enhancement in grayscale image processing. Each pixel in the grayscale image has a value ranging from 0 to 255, with different values corresponding to different levels of grayscale. In the context of mechanical diagnosis, image processing serves to facilitate feature extraction, and therefore, grayscale transformation or normalization can aid in subsequent calculations. Additionally, this method helps to mitigate the influence of illumination and background on fault feature extraction[50]. Grayscale transformation involves altering the gray value of the original image. For instance, in bearing diagnosis, Kapla et al.[51] utilize grayscale image conversion to extract features. Similarly, Xiao et al.[52] utilize gray image conversion to diagnose fan faults. The accuracy of image processing using a convolutional neural network has been observed to be close to 100%. Sun et al. analyze the SDP image after bearing signal conversion, employing grayscale and binarization processing. It is noted that this grayscale transformation method significantly reduces subsequent calculations[53]. Grayscale transformation is commonly categorized into three types: linear transformation, piecewise linear transformation, and nonlinear transformation. The formula for linear transformation is as follows:

$$g(x,y) = [\frac{d-c}{b-a}](f(x,y)-a)+c \tag{24}$$

Where *f*(*x*,*y*) is the pixel gray value of the original image in row *x* and column *y*, *g*(*x*,*y*) is the pixel gray value of the output image in row *x* and column, *a* is the minimum gray value of the original image, *b* is the maximum gray value of the original image, *c* is the minimum gray value of the output image, and *d* is the maximum gray value of the output image. In addition, the common linear transformation is image flipping. Within the range of [0, *L* - 1] gray level, the image flipping formula is as follows:

$$g(x,y) = L-1-f(x,y) \tag{25}$$

Where *L* represents the maximum gray value of the pixel.

Linear transformation alters the contrast of an image by adjusting the range of gray values in the output. The piecewise linear transformation partitions the image into distinct gray areas, enabling the transformation of each individual area. Fig. 7(a) illustrates the transformation relationship of the image through the piecewise function. The input image *f*(*x*,*y*) can be mapped to *g*(*x*,*y*) after undergoing the piecewise linear transformation. The figure demonstrates the possibility of transforming any grayscale range by manipulating the number of inflection points and the slope of the line.

$$g(x,y) = \begin{cases} (\frac{c}{a})f(x,y) & 0 \le f(x,y) < a \\ [\frac{d-c}{b-a}][f(x,y)-a]+c & a \le f(x,y) \le b \\ [\frac{N-d}{M-b}][f(x,y)-b]+d & b < f(x,y) \le M \end{cases} \tag{26}$$

Where *N* is the maximum gray value of the enhanced image, and *M* is the maximum gray value of the original image.

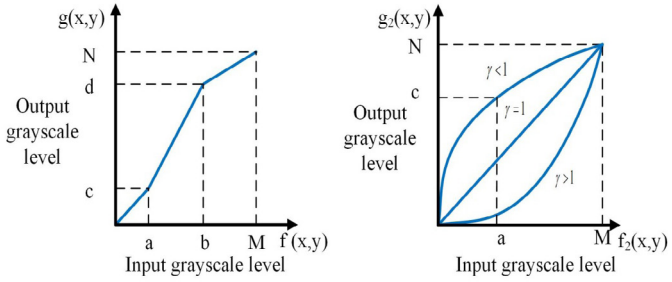

(a). Piecewise gray transform **(b). Logarithmic gray transform**

Figure 7: Principle diagram of nonlinear grayscale transformation

Linear transformation involves scaling the value of each pixel in the image. Consequently, linear transformation affects the entire gray range of the image in a linear manner. Nonlinear transformation involves mapping a nonlinear relationship between the output and input gray values. Nonlinear transformation can alter different gray scale ranges to varying degrees. For instance, the logarithmic transformation can be represented by the following formula:

$$g(x,y) = c * log(1+f(x,y)) \tag{27}$$

where is a constant. *f*(*x*,*y*) represents the pixel value of the original image, and *g*(*x*,*y*) represents the pixel value of the converted image.

Fig. 7(b) illustrates the suitability of performing a logarithmic conversion on the image's grayscale. The curve of the logarithmic function reveals that the pixel's gray value can be mapped to a wider gray value range in the middle. Exponential transformation is another type of nonlinear transformation that involves modifying the pixel values of the original image using the exponential function. The formula for exponential transformation can be expressed as:

$$g(x,y) = cf^{\gamma}(x,y) \tag{28}$$

Where *f*(*x*,*y*) represents the pixel value at (*x*,*y*). γ represents the order.

In the exponential function image, a γ value of 1 corresponds to a linear transformation. Increasing the γ value results in a decrease in the input pixel's gray value, compression of the low grayscale areas, stretching of the high grayscale areas, enhancement of the low grayscale values, and a brighter image. When the γ value is less than 1, the opposite occurs. The former method processes each pixel individually, while histogram enhancement transforms the same gray value uniformly. The histogram is divided into gray, gradient, and optical flow histograms, providing insight into the image's brightness

characteristics. The horizontal axis ranges from 0 to 255, representing the gray values, while the vertical axis represents the frequency or count of those gray values in the image. A larger proportion of low gray values indicates a darker image. Common image enhancement methods based on histograms include histogram equalization and histogram specification. The transformation equation for histogram-based image enhancement is shown in eq. 29.

$$g(x,y) = \begin{cases} E \cdot f(x,y) & if\ m_{S_{xy}} \le k_0 m_f\ AND\ k_1\sigma_f \le \sigma_{S_{xy}} \le k_2\sigma_f \\ f(x,y) & otherwise \end{cases} \quad (29)$$

Where σ_f is the standard deviation of the input image, m is the local mean, and E, K_0, K_1 and K_2 are the specified parameters.

According to the formula provided, the image can be enhanced through histogram manipulation, allowing for a comparison between local and global contrast. This comparison enables the adjustment of local pixel values by a factor of E. Unlike the simple function transformation method, histogram enhancement takes into consideration all images and local images simultaneously, processing similar pixels based on the regions that require improvement. Li et al.[54] utilized a histogram equalization algorithm to enhance image contrast, resulting in higher recognition accuracy in diagnosing faults of rotating machinery. Hameed et al.[55] applied a histogram-based approach to extract fault features in diagnosing planetary gearbox faults. Different fault types exhibit discernible differences, which can be visualized and used as a basis for classification through histograms. Joshuva et al.[56] utilized histograms to extract vibration signal features, achieving enhanced accuracy in diagnosing generator blade faults and improving the overall diagnostic efficiency. Yang et al.[57] investigated histogram coding strategies for detecting mechanical speed changes, specifically in analyzing vibration signals, and confirmed its excellent performance through simulations and real-world signals. Dias et al.[58] proposed the use of a directional gradient histogram to detect broken bars in motor rotors, which effectively extracts features that facilitate better classification. Song et al. employed a histogram-based approach, coupled with Principal Component Analysis, to diagnose blower faults, enabling swift and efficient extraction of signals across any probability density. Additionally, histograms were used to replace traditional parameters and generate new features through the integration of histograms and genetic programming, leading to improved diagnostic sensitivity[59, 60]. Sun et al.[61] employed the histogram of directional gradient features to enhance the ability of extracting fault features, mitigating the impact of limited grayscale and texture on feature extraction. Tayyab et al.[62] utilized Histograms of Oriented Grains (HOG) and Local Binary Patterns (LBP) to extract rolling bearing features from vibration images, which can be manually generated. Ding et al.[63, 64] utilized histograms to establish the relationship between bearing time-frequency images and time-frequency manifolds, demonstrating reliable performance in handling continuous noise. Chen et al.[65] represented different gear failures through histograms, which effectively depict the distinctions between various feature parameters.

Image feature enhancement based on convolutional neural network

In recent years, convolutional network technology has significantly advanced and found widespread applications in image processing. The powerful learning capabilities of neural networks have greatly contributed to image classification. In the field of fault diagnosis, such as crack detection, the primary approach is to extract meaningful features automatically from the image in order to eliminate interference from noise[66]. Consequently, CNN-based image feature extraction methods resemble filtering methods, seeking to filter out image noise and emphasize useful information. With the progress of machine vision, deep learning has made inroads into mechanical fault diagnosis owing to its ability to address highly complex problems. Converting a signal into a two-dimensional image for intuitive analysis and employing CNN-based diagnosis extraction outperforms traditional methods. Wang et al. transformed the vibration signal of a bearing into a two-dimensional RGB image, utilized a CNN-based convolutional network to extract image features, and subsequently diagnosed the bearing fault[67].

In machine image processing, images are commonly represented as matrices, with each pixel corresponding to a numerical value in the matrix. In convolutional neural networks, by computing and classifying this numerical matrix, the network achieves the desired denoising and classification effects. A typical convolutional neural network structure comprises several layers, including the convolution layer, activation function, pooling layer, fully connected layer, and output layer, as shown in fig. 8. Each layer serves a distinct purpose. The convolution layer is responsible for extracting features from images. In contrast to traditional filtering methods, the convolution layers leverage different objective functions to achieve diverse image feature extraction outcomes. Multiple pooling layers compress image data, thereby reducing network parameters. The fully connected layer is responsible for image classification. Hence, modifying the structure of the convolutional network can yield different image processing outcomes.

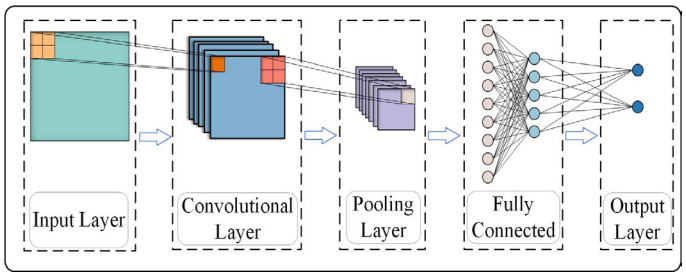

Figure 8: Convolution neural network flow chart

To address image noise, Quan et al.[68] enhanced the convolutional neural network by incorporating complex transformations, resulting in improved denoising effectiveness. The adoption of complex neural networks stems from their ability to express image features more effectively. As the image matrix resides within a two-dimensional space, the complex domain provides superior representation compared to the real field. Two-dimensional complex filters also outperform real filters. The complex domain convolutional denoising network structure is presented in fig. 9. Leveraging multi-layer convolution, the nonlinear activation function ReLU, and residual blocks, the network achieves image denoising. The convolution method no longer revolves around real number field convolution, but complex number field convolution, as formulated in eq.30. The rectified linear element function in the complex number field is depicted in eq.31, and the complex field normalization module is illustrated in eq.32.

$$A * K = (R(A) * R(K) - S(A) * S(K)) + (R(A) * S(K) + S(A) * S(K))i \quad (30)$$

$$CReLU(z) = ReLU(R(z)) + i \cdot ReLCU(S(z)) \quad (31)$$

$$BN(z) = ReBN(R(z)) + i \cdot ReBn(s(z)) \quad (32)$$

where R is the real part, S is the imaginary part, and $ReBN$ is the standard batch normalization with real-valued input.

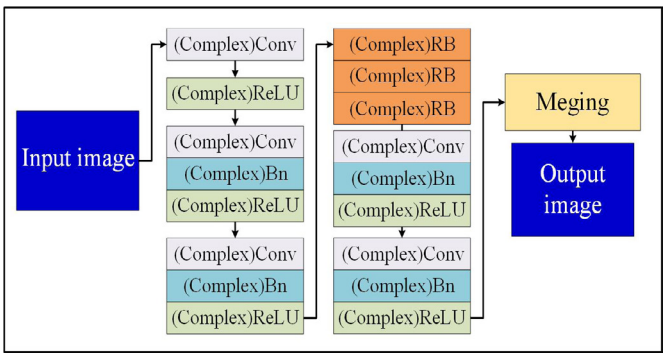

Figure 9: Image Enhancement of convolution Neural Network based on complex Domain

Applying convolution network transformations in a complex domain yields favorable denoising results, particularly in the removal of additive white Gaussian noise. Correspondingly, various improved convolutional neural network schemes have been devised to cater to diverse image processing objectives, as summarized in Table 3.

Table 3. Image enhancement method based on improved convolutional neural network

No	Method	Advantage	Ref
1	A multi-scale information fusion layer is added in front of the convo-lution layer of the traditional CNN to form a 2D multi-scale cascade CNN	Adapt to frequent changes in speed and load bearing diagno-.sis	69
2	The SE-CNN is formed by com-bining the channel attention mecha-.nism of SE network and CNN	Good generalization .ability and stability	70
3	Fault diagnosis task and signal de-noting task are integrated into CNN .to form JL-CNN	Good bearing fault diagnosis ability un-.der strong noise	71
4	Combining the generalization abil-ity of CNN and support vector ma-.chine, CNN-SVM is formed	Bearing diagnosis takes less time and .has high accuracy	72
5	CGAN-2-D-CNN is formed by combining conditional generative .adaptive network and CNN	The number of data samples for bearing .diagnosis is reduced	73

In summary, grayscale images are extensively employed in fault diagnosis due to their ease of calculation and analysis. In fault diagnosis, the grayscale distribution of an image can be altered through grayscale transformation and histogram techniques, which enhance the original image information and improve its visual clarity. The selection of an appropriate grayscale transformation method effectively accentuates the image's feature information, thereby facilitating fault diagnosis in rotating machinery.

Image feature enhancement based on fusion

Multi-spectral image fusion is a widely-used approach in mechanical fault diagnosis. For instance, in power equipment, thermal defects contribute to as much as 90% of equipment failures. Hence, by merging infrared and visible images, it is possible to determine the location of faults, estimate the remaining lifespan, and diagnose the fault type. Consequently, image fusion plays a crucial role in the field of fault diagnosis, and the classification of fusion methods is illustrated in **fig. 10**.

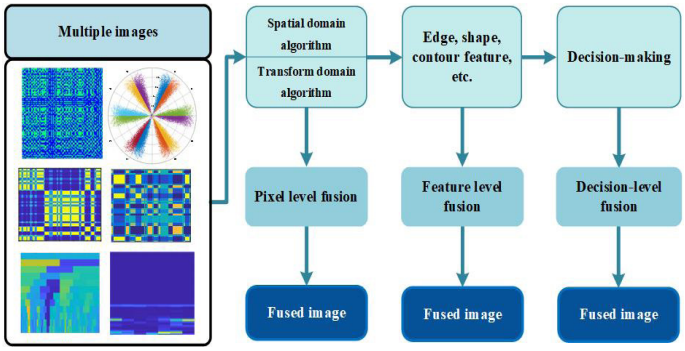

Figure 10: Image fusion method

Prior to image fusion, it is essential to register the images in order to facilitate the fusion of regions containing similar information. This process requires the extraction of image feature areas or the measurement of pixel intensity. Yang et al.[74] classify and match the edge feature points of power equipment to accomplish the fusion of multi-spectral images. To establish a standard image library, both the infrared and visible images of normal equipment are utilized. The global edge contour correlation coefficient between the standard infrared image and the infrared detection image is calculated using normalized cross correlation, resulting in the creation of a template image. Subsequently, the improved speeded-up robust features method is employed for the secondary recognition of image features, aiming to eliminate background noise and interference from other equipment components. The secondary recognition method primarily relies on comparing Euclidean distances and applying the minimum principle of the cost function to extract the region for image fusion.

In fault diagnosis, various types of images are used for data conversion, promoting the development of multi-image fusion. Recursive plots, due to their symmetry, often contain redundant information (eq. 33). Zhang et al.[75] employed this method to fuse various recursive plots. The recursive plot is based on its diagonal symmetry property. The long sequence signal is divided into two parts, and each group is converted into a recursive plot. Image fusion is achieved by combining two diagonal matrices (fig. 11). This method mitigates information redundancy and effectively highlights the features of long sequence signals. Nath et al.[76] also utilized a recursive plot for fusion, where they fused three recursive plots into a three-dimensional image. This image fusion method facilitates the analysis of time series. Kim et al.[77] similarly employed three images for fusion, but not by simply superimposing them. They utilized the principle of three RGB channels to convert the images into channel values, generating color images. Experimental results have shown the method's good classification accuracy for signals. In the image fusion process, Ying et al.[78] introduced the method of interpolation compensation error to enhance the quality of incompletely registered images. Firstly, spatial sampling and spectral mapping are employed, followed by the use of LR-HIS to generate HR-MSI. The edge difference (ED) is calculated for LR and HR images with varying pixel values. A smaller ED indicates a better image alignment (eq. 34).

$$RP_{i,j}(e) = \Theta(\epsilon - ||\vec{x}(i) - \vec{x}(j)||), \quad \vec{x}(\cdot) \in \mathcal{R}^m, i, j = 1, \cdots, N, \quad (33)$$

Where $RP_{i,j}$ represents the recursive pixel value. $\vec{x}(i)$ represents the ith state of phase space. Θ Represents a function

of thresholding a matrix. **ε** is the threshold. *m* is the number of points in each state of the phase space. represents the total number of states.

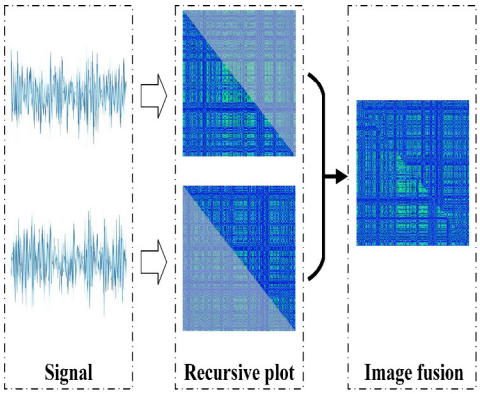

Figure 11: Recursive plot diagonal fusion

$$ED(I_c, I_b) = \sum_j |E_C - E_b|_1 \quad (34)$$

Where I_c and I_b are clear images and fuzzy images respectively, E_C and E_b are edges of clear images and fuzzy images respectively. The calculation expression of E is shown in eq.35.

$$E(x, y, j) = \sqrt{\partial_x^2 I(x, y, j) + \partial_y^2 I(x, y, j)} \quad (35)$$

Where (x,y) is the location coordinate of the pixel, j is the image band.

The different images are then registered using the minimum normalized edge difference, as described by the calculation method in eq.36. In order to mitigate the problem of local optimization, the registration accuracy and speed are improved by employing the edge image pyramid. In the image fusion process, the spectral basis matrix is computed and the coefficient matrix is solved to fuse the images, as demonstrated in eq.37.

$$NED(I_c, I_b) = \frac{\sum_j \|E_c - E_b\|_1}{\sum_j (\|E_c\|_1 + \|E_b\|_1)}, A = arcsinJ(A) \quad (36)$$

where $J(A) = NDE(I_c(\mathcal{T}(X, A)), I_b(X))$, $A_0 = (1,0,0,0,1,0)^T$, $A^{t+1} = A^t - \gamma \nabla_A^t J$.

The different images are then registered using the minimum normalized edge difference, as described by the calculation method in eq.36. In order to mitigate the problem of local optimization, the registration accuracy and speed are improved by employing the edge image pyramid. In the image fusion process, the spectral basis matrix is computed and the coefficient matrix is solved to fuse the images, as demonstrated in eq.37.

$$Z = VE \quad (37)$$

Where V represents spectral basis matrix, E as the coefficient matrix.

$$E = argmin\Psi(E) = argmin \| X - VES \|_F^2 + n \| X - RE \|_F^2 + \gamma \| E \|_F^2 \quad (38)$$

Where S is the spatial mapping matrix E stands for coefficient matrix. V denotes the spectral basis matrix. R and B are parameters determined by the sensor.

The fusion of images effectively addresses the registration problem and enhances the overall image quality. In fault diagnosis, this lays a solid foundation for subsequent image processing. The accuracy of image registration significantly impacts the quality of image fusion, which enables superior display of signal information across various dimensions. Increased feature information in fault diagnosis leads to improved classification accuracy. The image fusion method combines diverse image features, effectively merging the features from different images into a single image. This significantly simplifies the computational complexity. Additionally, the image fusion algorithm offers a novel avenue for enhancing image features to a certain extent.

Image feature enhancement based on segmentation

Image segmentation technology has found widespread use in various domains, including natural science, medicine, remote sensing, and industrial applications[79]. It is particularly valuable when the feature information is localized within specific areas of an image, as it allows for the extraction and highlighting of these feature regions. By employing image segmentation, the volume of image data can be reduced, which facilitates subsequent higher-level processing and analysis. The accuracy of image segmentation directly impacts the quality of the subsequent processing stage, making it a focal point of research. Currently, the primary methods for image segmentation include threshold-based, region-based, edge-based, and super-pixel segmentation techniques.

Image segmentation is a method of data feature extraction that can be applied to image data, represented as a two-dimensional matrix. Song et al.[80] utilized a data conversion technique to extract fault features from a rotating motor. They employed an unsupervised sequence segmentation approach based on a convolutional neural network to highlight signal features, enabling early fault detection. Similarly, Yu et al.[81] utilized machine vision image processing techniques to detect bearing faults. They employed adaptive threshold segmentation and the Canny edge detection method to accurately segment bearing surface defects. This approach reduces noise influence, shortens diagnosis time, and enhances detection accuracy through contrast enhancement. Yun et al.[82] proposed a data enhancement method for diagnosing planetary bearings. They applied overlapping segmentation methods to enhance vibration data and incorporated dictionary learning to improve fault classification accuracy. Experimental results demonstrated high anti-noise capability. Zhao et al.[83] reshaped signals into segmentation matrices using a segmentation method. They extracted feature frequencies by stacking them into three-stage tensors and conducted wind turbine bearing analysis. This method effectively extracts fault features and separates fault sources. Furthermore, Zhao et al. [84] proposed an adaptive defect region segmentation algorithm for detecting defects in universal joint bearings. This algorithm accurately segments the defect area and exhibits good recognition accuracy in dealing with bearing surface defects. It is also applicable in practice due to its processing speed. Moreover, Khodja[85] utilized a time-moving segmentation window to segment temporal vibration signals, enabling bearing fault diagnosis at different speeds. The proposed method demonstrates high accuracy and robustness even in the presence of noise.

Currently, there is a lack of a specific theoretical framework to guide the selection of appropriate methods, resulting in the reliance on methods tailored to specific image types for more effective processing. Nevertheless, image segmentation undeniably plays a crucial role in feature extraction. It enables the removal of redundant information from images and emphasizes their distinctive features. Various image segmentation methods yield different outcomes, even at the same processing speed.

In fault diagnosis, there is a need to strike a balance between accuracy and speed. Enhancing processing speed is also a crucial aspect of advancing image segmentation technology.

Future Trends and Remarks

The analysis and synthesis of existing literature lead to the following conclusions: A majority of the literature focuses on image-based fault diagnosis methods, which have been extensively utilized in fault diagnosis applications. Filtering-based image enhancement methods effectively reduce image noise. Template-based methods enhance image features through various means, such as texture feature enhancement, smooth image generation, and filtering. Gray-based image enhancement methods modify the gray distribution of the image to highlight feature information using different grayscale conversion approaches. Convolutional neural network-based image enhancement methods demonstrate a diverse range of techniques. Image fusion-based enhancement methods combine information from multiple images to improve overall image quality. Image segmentation techniques are employed to isolate specific areas of an image, making it possible to select fault regions.

Image enhancement methods play a vital role in image-based fault diagnosis, offering various techniques suitable for different diagnostic purposes. To further enhance the accuracy and efficiency of diagnosis, the following areas warrant further investigation:

Fusion of multiple image enhancement techniques is essential in the field of fault diagnosis. Image enhancement techniques often have both benefits and drawbacks. After image processing, the relevant information is typically filtered or masked. However, using various enhancement methods can affect the speed of image processing. Effectively extracting useful information from data remains an essential aspect of fault diagnosis.

Enhancing the efficiency of image enhancement is crucial in reducing the complexity of image processing. Images contain a vast amount of information, which often leads to intricate processing requirements. A key future objective is to improve the speed of image processing in fault diagnosis, as this will significantly reduce diagnosis time.

Investigate a novel treatment approach. Typically, fault diagnosis relies on simplistic image processing methods, which may not yield optimal outcomes. Thus, enhancing both the accuracy and efficiency of fault diagnosis requires a deeper understanding of how images impact the process.

Within the realm of image-based fault diagnosis, numerous image processing methods exist, making it challenging to determine the most suitable one. Since the effects of various methods vary, it is crucial to explore the selection of appropriate processing methods based on different image types.

Future research opportunities can be explored in the following areas: enhancing the accuracy of diagnosis by highlighting fault-prone features through image enhancement, and advancing the development of fast and efficient image processing methods to address the evolving requirements of fault diagnosis. High-speed image processing enables rapid data processing, enhanced fault information extraction, and increased throughput in detection data.

In the field of rotating machinery, fault diagnosis outcomes are influenced by factors such as rotating frequency and load. Investigating the application of images to address fault diagnosis at various frequencies represents a novel research direction. Noise often disrupts signals in the diagnosis of rotating machinery, masking crucial fault features and complicating the diagnostic process. Image feature enhancement can mitigate the impact of strong noise conditions, offering practical research significance.

Purposeful image enhancement is necessary to effectively highlight variations between different faults. This method can be extended for more complex fault diagnosis scenarios. Furthermore, incorporating cross-domain knowledge from other image processing methods can enhance the diagnostic capacity of rotating machinery equipment by integrating new image processing technologies.

Conclusion

Image feature enhancement is a useful approach in fault diagnosis with images. Therefore, this paper aims to elucidate the image feature extraction method in the domain of rotating machinery. This review summarizes various image enhancement methods that primarily focus on diagnosing faults in rotating machinery. Additionally, this paper presents novel approaches to image processing, specifically filtering, templates, and grayscale transformation. Furthermore, the paper provides a brief introduction to image fusion and image segmentation methods. Finally, the challenges and difficulties associated with image feature enhancement techniques in fault diagnosis are discussed. Considering the characteristics of rotating machinery, potential research directions for the future are proposed. The paper concludes by summarizing the application of image feature enhancement to rotating machinery and highlighting the effectiveness of using images for fault signal classification. Overall, this article serves as a reference for further research and development in fault diagnosis for rotating machinery.

References

1. Liu X, Zhao X, He K. Feasibility Study of the GST-SVD in Extracting the Fault Feature of Rolling Bearing under Variable Conditions. Chinese Journal of Mechanical Engineering, 2022, 35(1):133.
2. Liu Z, Xu M, Zhang H, et al. Nonlinear dynamic analysis of variable lead preloaded single nut ball screw considering the variation of working parameters. Nonlinear Dynamics, 2022, 108(1):141-166.
3. Zhang J, Han D, Song M, Xie, Z Rao, Z, Donglin Zou. Theoretical and experimental investigation on the effect of supply pressure on the nonlinear behaviors of the aerostatic bearing-rotor system. Mechanical Systems and Signal Processing, 2021, 158:107775.
4. Tang Y, Zhang X, Qin G, et al. Graph Cardinality Preserved Attention Network for Fault Diagnosis of Induction Motor Under Varying Speed and Load Condition. IEEE Transactions on Industrial Informatics, 2021, 18(6):3702-3712.
5. Li Q, Li S, Wu P, et al. Investigation on reduction of pressure fluctuation for a double-suction centrifugal pump. Chinese Journal of Mechanical Engineering, 2021, 34:1-18.
6. Li Q, Ding X, He Q, et al. Manifold sensing-based convolution sparse self-learning for defective bearing morphological feature extraction. IEEE Transactions on Industrial Informatics, 2020, 17(5):3069-3078.
7. Liu J, Xu Y, Pan G. A combined acoustic and dynamic model of a defective ball bearing. Journal of Sound and Vibration, 2021, 501:116029.

8. Dong Y, Pan Y, Wang D, et al. Corrosion detection and evaluation for steel wires based on a multi-vision scanning system. Construction and Building Materials, 2022, 322:125877.
9. Long Z, Zhang X, He M, et al. Motor fault diagnosis based on scale invariant image features. IEEE Transactions on Industrial Informatics, 2021, 18(3):1605-1617.
10. Liu X, Miao X, Jiang H, et al. Box-point detector: A diagnosis method for insulator faults in power lines using aerial images and convolutional neural networks. IEEE Transactions on Power Delivery, 2021, 36(6):3765-3773.
11. Ma Y, Liu J, Liu Y, et al. Structure and illumination constrained GAN for medical image enhancement. IEEE Transactions on Medical Imaging, 2021, 40(12): 3955-3967.
12. Yan P, Liu X, Wang F, et al. LOVD: Land Vehicle Detection in Complex Scenes of Optical Remote Sensing Image. IEEE Transactions on Geoscience and Remote Sensing, 2021, 60:1-13.
13. Zhao R, Shi Z, Zou Z. High-resolution remote sensing image captioning based on structured attention. IEEE Transactions on Geoscience and Remote Sensing, 2021, 60:1-14.
14. Zhang Y, Di X, Zhang B, et al. Better Than Reference in Low-Light Image Enhancement: Conditional Re-Enhancement Network. IEEE Transactions on Image Processing, 2021, 31:759-772.
15. Li Z, Qiao F, Lu W, et al. Vibration Characteristics of Rotor System with Loose Disc Caused by the Insufficient Interference Force. Chinese Journal of Mechanical Engineering, 2022, 35(1):1-15.
16. Kumar R, Bhandari A K. Fuzzified contrast enhancement for nearly invisible images. IEEE Transactions on Circuits and Systems for Video Technology, 2021, 32(5): 2802-2813.
17. Srinivas K, Bhandari A K, Kumar P K. A context-based image contrast enhancement using energy equalization with clipping limit. IEEE Transactions on Image Processing, 2021, 30:5391-5401.
18. Yuan J, Cao W, Cai Z, et al. An underwater image vision enhancement algorithm based on contour bougie morphology. IEEE Transactions on Geoscience and Remote Sensing, 2020, 59(10):8117-8128.
19. Huang H, Yang W, Hu Y, et al. Towards low light enhancement with raw images. IEEE Transactions on Image Processing, 2022, 31:1391-1405.
20. Hong D, Wu X, Ghamisi P, et al. Invariant attribute profiles: A spatial-frequency joint feature extractor for hyperspectral image classification. IEEE Transactions on Geoscience and Remote Sensing, 2020, 58(6):3791-3808.
21. Xie T, Huang X, Choi S K. Intelligent Mechanical Fault Diagnosis Using Multisensor Fusion and Convolution Neural Network. IEEE Transactions on Industrial Informatics, 2021, 18(5):3213-3223.
22. Xiao B, Yin S. A deep learning based data-driven thruster fault diagnosis approach for satellite attitude control system. IEEE Transactions on Industrial Electronics, 2020, 68(10):10162-10170.
23. Shao H, Xia M, Han G, et al. Intelligent fault diagnosis of rotor-bearing system under varying working conditions with modified transfer convolutional neural network and thermal images. IEEE Transactions on Industrial Informatics, 2020, 17(5):3488-3496.
24. Kaya Y, Kuncan M, Kaplan K, et al. Classification of bearing vibration speeds under 1D-LBP based on eight local directional filters. Soft Computing, 2020, 24(16):12175-12186.
25. Wang B, Ding, C. Transient feature identification from internal encoder signal for fault detection of planetary gearboxes under variable speed conditions. Measurement 171 (2021):108761.
26. Zhang Z, Li S, Lu J, Wang J, Jiang, X. A novel intelligent fault diagnosis method based on fast intrinsic component filtering and pseudo-normalization. Mechanical Systems and Signal Processing 145 (2020):106923.
27. Li W, Shang Z, Qian S, Zhang B, Zhang J, Gao M. A novel intelligent fault diagnosis method of rotating machinery based on signal-to-image mapping and deep Gabor convolutional adaptive pooling network. Expert Systems with Applications (2022):117716.
28. Zou F, Zhanget H, Sang S, Li X, He W, Liu X. Bearing fault diagnosis based on combined multi-scale weighted entropy morphological filtering and bi-LSTM. Applied Intelligence 51.10 (2021):6647-6664.
29. Yahaghi E, Mirzapour M, Movafeghi A, Rokrok, B. Interlaced bilateral filtering and wavelet thresholding for flaw detection in the radiography of weldments. The European Physical Journal Plus 135.1 (2020):1-10.
30. Figlus T. A method for diagnosing gearboxes of means of transport using multi-stage filtering and entropy. Entropy 21.5 (2019):441.
31. Ghosh S, Gavaskar RG, Panda D, Chaudhury KN. Fast scale-adaptive bilateral texture smoothing. IEEE Transactions on Circuits and Systems for Video Technology 30.7 (2019):2015-2026.
32. Li J, Ding W, Zhang J, Tao J. Period-assisted adaptive parameterized wavelet dictionary and its sparse representation for periodic transient features of rolling bearing faults. Mechanical Systems and Signal Processing 169 (2022):108796.
33. Nair P, Chaudhury KN. Fast high-dimensional kernel filtering. IEEE Signal Processing Letters, 2019, 26(2):377-381.
34. Young SI, Girod B, Taubman D. Gaussian lifting for fast bilateral and nonlocal means filtering. IEEE Transactions on Image Processing, 2020, 29:6082-6095.
35. Geng J, Jiang W, Deng X. Multi-scale deep feature learning network with bilateral filtering for SAR image classification. ISPRS Journal of Photogrammetry and Remote Sensing, 2020, 167:201-213.
36. Wang Q, Wang X, Fang C, Yang, W. Robust fuzzy c-means clustering algorithm with adaptive spatial & intensity constraint and membership linking for noise image segmentation. Applied Soft Computing 92 (2020):106318.
37. Manno D, Cipriani G, Ciulla G, Dio VD, Guarino S, Brano VL. Deep learning strategies for automatic fault diagnosis in photovoltaic systems by thermographic images. Energy Conversion and Management 241 (2021):114315.
38. Al-Musawi AK, Anayi F, Packianather M. Three-phase induction motor fault detection based on thermal image segmentation. Infrared Physics & Technology, 2020, 104:103140.
39. Long H, Xu S, Gu W. An abnormal wind turbine data cleaning algorithm based on color space conversion and image feature detection. Applied Energy, 2022, 311:118594.
40. Chen Y, Song B, Zeng Y, Du X, Guizani M. A deep learning-based approach for fault diagnosis of current-carrying ring in catenary system. Neural Computing and Applications (2021):1-13.
41. Jiang Z, Li H, Liu L, Men A, Wang H. A switched view of retinex: deep self-regularized low-light image enhancement. Neurocomputing 454 (2021):361-372.
42. Xu J, Hou Y, Ren D et al. Star: A structure and texture aware retinex model. IEEE Transactions on Image Processing 29 (2020):5022-5037.
43. Tang M, Xie F, Zhang R, Jiang Z, Bovik AC. A local flatness based variational approach to retinex. IEEE Transactions on Image Processing 29 (2020):7217-7232.

44. Li P, Tian J, Tang Y, Wang G, Wu C. Deep retinex network for single image dehazing. IEEE Transactions on Image Processing 30 (2020):1100-1115.

45. Gu Z, Li F, Lv XG. A detail preserving variational model for image Retinex. Applied Mathematical Modelling, 2019, 68:643-661.

46. Lecca M, Rizzi A, Serapioni RP. An image contrast measure based on Retinex principles. IEEE Transactions on Image Processing, 2021, 30:3543-3554.

47. Zhou Z, Feng Z, Liu J, Hao, S. Single-image low-light enhancement via generating and fusing multiple sources. Neural Computing and Applications, 2020, 32:6455-6465.

48. Gu Z, Li F, Fang F, Zhang G. A novel retinex-based fractional-order variational model for images with severely low light. IEEE Transactions on Image Processing, 2019, 29:3239-3253.

49. Li J, Lu Y, Shen N, Pu J, Ma Z. Adaptive image enhancement and dynamic-template-matching-based edge extraction method for diamond roller on-machine profile measurement. The International Journal of Advanced Manufacturing Technology, 2022, 120(9-10):5997-6010.

50. Glowacz A. Fault diagnosis of electric impact drills using thermal imaging. Measurement, 2021, 171:108815.

51. Kaplan K, Kaya Y, Kuncan M, Minaz, MR, Ertunç HM. An improved feature extraction method using texture analysis with LBP for bearing fault diagnosis. Applied Soft Computing, 2020, 87:106019.

52. Xiao W, Ye Z, Wang S. Fault Diagnosis of Wind Turbine Based on Convolution Neural Network Algorithm. Computational Intelligence and Neuroscience, 2022, 2022.

53. Sun Y, Li S, Wang X. Bearing fault diagnosis based on EMD and improved Chebyshev distance in SDP image. Measurement, 2021, 176:109100.

54. Zou L, Lam HF, Hu J. Adaptive resize-residual deep neural network for fault diagnosis of rotating machinery. Structural Health Monitoring, 2022:14759217221122266.

55. Hameed SS, Muralidharan V, Ane BK. Comparative analysis of fuzzy classifier and ANN with histogram features for defect detection and classification in planetary gearbox. Applied Soft Computing, 2021, 106:107306.

56. Joshuva A, Sugumaran V. A lazy learning approach for condition monitoring of wind turbine blade using vibration signals and histogram features. Measurement, 2020, 152:107295.

57. Yang S, Lu G, Wang A, Jie L, Peng Y. Change detection in rotational speed of industrial machinery using Bag-of-Words based feature extraction from vibration signals. Measurement, 2019, 146:467-478.

58. Dias CG, da Silva LC, Alves WAL. A histogram of oriented gradients approach for detecting broken bars in squirrel-cage induction motors. IEEE Transactions on Instrumentation and Measurement, 2020, 69(9):6968-6981.

59. Song L, Wang H, Chen P. Automatic signal quality check and equipment condition surveillance based on trivalent logic diagnosis theory. Measurement, 2019, 136: 173-184.

60. Song L, Wang H, Chen P. Intelligent diagnosis method for machinery by sequential auto-reorganization of histogram. ISA transactions, 2019, 87:154-162.

61. Sun W, Cao X. Curvature enhanced bearing fault diagnosis method using 2D vibration signal. Journal of Mechanical Science and Technology, 2020, 34(6):2257-2266.

62. Tayyab S M, Chatterton S, Pennacchi P. Image-Processing-Based Intelligent Defect Diagnosis of Rolling Element Bearings Using Spectrogram Images. Machines, 2022, 10(10):908.

63. Hao S, Han X, Guo Y, Xu X, Wang, M. Low-light image enhancement with semi-decoupled decomposition. IEEE transactions on multimedia 22.12 (2020): 3025-3038.

64. Ding X, He Q, Shao Y, Huang W. Transient feature extraction based on time–frequency manifold image synthesis for machinery fault diagnosis. IEEE Transactions on Instrumentation and Measurement 68.11 (2019): 4242-4252.

65. Chen C, Shen, F, Xu J, Yan R. Probabilistic latent semantic analysis-based gear fault diagnosis under variable working conditions. IEEE Transactions on Instrumentation and Measurement 69.6 (2019): 2845-2857.

66. Bang S, Park S, Kim H, Kim H. Encoder–decoder network for pixel-level road crack detection in black-box images. Computer-Aided Civil and Infrastructure Engineering 34.8 (2019): 713-727.

67. Wang Z, Zhao W, Du W, Li N, Wang J. Data-driven fault diagnosis method based on the conversion of erosion operation signals into images and convolutional neural network. Process Safety and Environmental Protection 149 (2021): 591-601.

68. Quan Y, Chen Y, Shao Y, Teng H, Xu Y, Ji H. Image denoising using complex-valued deep CNN. Pattern Recognition 111 (2021): 107639.

69. Zhang L, Lv Y, Huang W, Yi C. Bearing fault diagnosis under various operation conditions using synchrosqueezing transform and improved two-dimensional convolutional neural network. Measurement Science and Technology 33.8 (2022): 085002.

70. Wang H, Xu J, Yan R, Gao RX. A new intelligent bearing fault diagnosis method using SDP representation and SE-CNN. IEEE Transactions on Instrumentation and Measurement 69.5 (2019):2377-2389.

71. Wang H, Liu Z, Peng D, Cheng Z. Attention-guided joint learning CNN with noise robustness for bearing fault diagnosis and vibration signal denoising. ISA transactions 128 (2022):470-484.

72. Han T, Zhang L, Yin Z, Tan ACC. Rolling bearing fault diagnosis with combined convolutional neural networks and support vector machine. Measurement 177 (2021):109022.

73. Yang J, Liu J, Xie J, Wang C, Ding T. Conditional GAN and 2-D CNN for Bearing Fault Diagnosis With Small Samples. IEEE Transactions on Instrumentation and Measurement 70 (2021):1-12.

74. Pan H, Jing Z, Leung H, Li M. Hyperspectral image fusion and multitemporal image fusion by joint sparsity. IEEE Transactions on Geoscience and Remote Sensing 59.9 (2020):7887-7900.

75. Zhang Y, Hou Y, Yang KO, Zhou S. Multi-scale signed recurrence plot based time series classification using inception architectural networks. Pattern Recognition 123 (2022):108385.

76. Nath AG, Udmale SS, Raghuwanshi D, Singh SK. Improved structural rotor fault diagnosis using multi-sensor fuzzy recurrence plots and classifier fusion. IEEE Sensors Journal, 2021, 21(19):21705-21717.

77. Kim Y, Kim T, Youn, BD, Ahn S-H. Machining quality monitoring (MQM) in laser-assisted micro-milling of glass using cutting force signals: an image-based deep transfer learning. Journal of Intelligent Manufacturing 33.6 (2022):1813-1828.

78. Ying J, Shen H L, Cao S Y. Unaligned hyperspectral image fusion via registration and interpolation modeling. IEEE Transactions on Geoscience and Remote Sensing, 2021, 60:1-14.

79. Czerniawski T, Leite F. Automated segmentation of RGB-D images into a comprehensive set of building components using deep learning. Advanced Engineering Informatics, 2020, 45:101131.

80. Song W, Shen W, Gao L, Li X. An early fault detection method of rotating machines based on unsupervised sequence segmentation convolutional neural network. IEEE Transactions on Instrumentation and Measurement 71 (2021):1-12.

81. Dongling Y, Xiaohui Z, Jianzhen Z, Nanxing W. An enhancement algorithm based on adaptive updating template with Gaussian model for Si3N4 ceramic bearing roller surface defects detection. Ceramics International 48.5 (2022):6672-6680.

82. Kong Y, Qin Z, Han Q, Wang T, Chu F. Enhanced dictionary learning based sparse classification approach with applications to planetary bearing fault diagnosis. Applied Acoustics, 2022, 196:108870.

83. Zhao H, Zhang W. Fault diagnosis method for rolling bearings based on segment tensor rank-(Lr, Lr, 1) decomposition. Mechanical Systems and Signal Processing, 2019, 132:762-775.

84. Zhao Z, Hu B, Feng Y, et al. Multi-surface defect detection for universal joint bearings via multimodal feature and deep transfer learning. International Journal of Production Research (2022):1-17.

85. Khodja AY, Guersi N, Saadi MN, Boutasseta, N. Rolling element bearing fault diagnosis for rotating machinery using vibration spectrum imaging and convolutional neural networks. The International Journal of Advanced Manufacturing Technology 106.5 (2020):1737-1751.